

# FROM PIXELS TO PATCHES: 🏊 POOLING STRATEGIES FOR EARTH EMBEDDINGS\*

Isaac Corley<sup>λ</sup>, Caleb Robinson<sup>γ</sup>, Inbal Becker-Reshef<sup>γ</sup>, Juan M. Lavista Ferres<sup>γ</sup>

<sup>λ</sup>Wherobots, <sup>γ</sup>Microsoft AI for Good Research Lab

## ABSTRACT

As geospatial foundation models shift from patch-level to pixel-level embeddings, practitioners must aggregate thousands of pixel vectors into patch representations that preserve class-discriminative signal while matching downstream label resolution. The default choice, mean pooling, discards within-patch variability and can drop accuracy by more than 10% under spatial shift. To evaluate this effect, we introduce *EuroSAT-Embed*: 81,000 embedding GeoTIFFs derived from three foundation models: AlphaEarth, OlmoEarth, and Tessera. We benchmark 11 training-free and 2 parametric pooling methods under both random and geographically disjoint test splits. Our results show that richer pooling schemes reduce the geographic generalization gap by up to 40% relative to mean pooling and increases accuracy by up to 5% on spatial splits. We recommend Generalized Mean Pooling (GeM) as a drop-in replacement for mean pooling: it improves accuracy without increasing embedding dimensionality. For maximum accuracy, Stats pooling (concatenation of min/max/mean/std pooling) performs best at  $4\times$  the embedding size. We further find that pooling effectiveness varies across embedding sources and that higher-dimensional embeddings benefit most from distributional statistics.

## 1 INTRODUCTION

Geospatial foundation models (GFMs) turn satellite data time-series into embedding data products which can be reused across tasks and regions Fang et al. (2026). Recent GFMs create dense satellite imagery embeddings, i.e. at a *pixel* resolution, but many downstream tasks operate on objects or regions (fields, parcels, buildings, solar farms, gridded patches), requiring aggregation of pixel embeddings over polygons. Pooling (i.e. aggregation) is therefore an inherent step in using GFM output in these tasks, however naive methods may erase relevant signals in the embeddings.

This problem compounds when labels exist at a coarser-than-pixel resolution, known as the *input-label resolution mismatch* (Workman et al., 2023). For example, EuroSAT (Helber et al., 2019) contains  $64\times 64$  patches of 10 m pixels corresponding to a single land-cover label, which can be viewed as a *zonal-statistics* aggregation operation (Cressie, 2015). Unlike raw spectral bands, pixel embeddings encode semantic features that vary within a land-cover patch. This heterogeneity suggests that averaging can remove class signal that richer statistics keep. This makes pooling a design decision for geospatial applications with coarse labels and/or temporal dimensions.

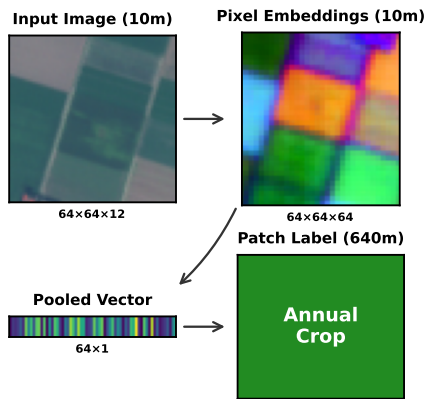


Figure 1: **Pixel-to-patch pooling.** The input-label resolution mismatch requires aggregating dense pixel embeddings (shown as PCA pseudo-RGB) to a lower resolution for downstream tasks.

\*No swimming required.

Pooling is underexplored for earth embeddings<sup>1</sup>, though it is heavily studied in related domains. In image retrieval, choices like generalized mean (GeM) pooling (Radenović et al., 2018) often matter as much as the learned encoder. In audio and video processing, statistical pooling (concatenating means and standard deviations) effectively summarizes variable-length sequences (Miech et al., 2017). Mean pooling dominates for its simplicity, but its performance under spatial shift is not well measured. Classical object-based image analysis (EO4GEO, 2026) methods like Bag of Visual Words (BoVW) (Csurka et al., 2004) aggregate hand-crafted features based on region statistics for vision tasks, but there is little work on aggregating modern pixel embeddings into patch-level representations.

In this paper, we focus on the pooling step; we benchmark 11 training-free methods and 2 parametric baselines using pixel embeddings generated by three GFM on the common EuroSAT land-cover classification dataset Helber et al. (2019). We evaluate the effects of pooling choice with kNN and linear probes of the EuroSAT embeddings under the standard random and geographically disjoint dataset splits.

Specifically, we release *EuroSAT-Embed*: three aligned pixel embedding datasets (81,000  $64 \times 64 \times D$  GeoTIFFs) enabling reproducible pooling research without re-running GFM inference. We run a comprehensive grid (3 encoders  $\times$  13 pools  $\times$  2 probes  $\times$  2 splits), and report tradeoffs between accuracy, generalization gaps, and size of the embedding dimension. We show that **GeM pooling improves spatial-split accuracy by +5% over mean pooling without increasing dimensionality**, while stats pooling reaches peak accuracy (+7–10%) at  $4 \times$  the embedding size. Parametric methods (PCA, BoVW) are inconsistent across embedding sources.

## 2 DATA AND EMBEDDINGS

**EuroSAT.** We use the 10-class EuroSAT land-cover dataset (Helber et al., 2019) which contains 27,000 Sentinel-2 patches at  $64 \times 64$  pixels with classes such as forest, residential, and agricultural land. We evaluate on both the standard random split (Neumann et al., 2019) and a spatial split (Ekim et al., 2025) that partitions samples by longitude to reduce train-test leakage via spatial autocorrelation.

**EuroSAT-Embed.** We construct three aligned embedding datasets from GFMs spanning embedding sizes: (1) *EuroSAT-AEF* uses AlphaEarth (Brown et al., 2025), which compresses annual satellite image time-series into 64-d embeddings per pixel quantized to `int8` (3.3 GB total); (2) *EuroSAT-OlmoEarth* uses OlmoEarth-Nano (Herzog et al., 2025), producing 128-d `float32` embeddings (40 GB); (3) *EuroSAT-Tessera* uses Tessera (Feng et al., 2025), encoding temporal surface spectra into 512-d `float32` embeddings (164 GB). AEF and OlmoEarth embed patch context but emit *pixel-wise* vectors, whereas Tessera encodes per-pixel time-series without spatial context of adjacent pixels. All datasets are aligned to EuroSAT’s 2018 imagery and released under CC-BY-4.0 at <https://hf.co/datasets/isaaccorley/eurosat-embed>.

## 3 POOLING METHODS

We benchmark training-free operators that compress an  $H \times W \times D$  embedding tensor into a  $d$ -dimensional vector. We hypothesize that class signal lies not only in the mean but in the distribution (variance and extremes). For example, a residential neighborhood might share a mean embedding over space with industrial areas, but show higher variance from mixed rooftops, vegetation, and roads. Let  $X \in \mathbb{R}^{H \times W \times D}$  denote a patch with  $N=HW$  pixels. Pooling operates per channel (e.g.,  $\max(X)$  returns the per-channel maximum). Note that pooling methods can increase the dimensionality by a multiplier, see the `Dim $\times$`  column reported in Tables 1, 2, due to concatenation of multiple statistics.

**First-order statistics** ( $D$ -d each): *mean* ( $\mu = \frac{1}{N} \sum_i x_i$ ) captures the “typical” pixel but discards variation; *max* preserves extreme activations; generalized mean (*GeM*,  $p=3$ ) interpolates between them (Radenović et al., 2018); *center-weighted mean* applies a Gaussian ( $\sigma = \min(H, W)/4$ ) to down-weight boundary pixels.

<sup>1</sup>A relevant exception is the recent OlmoEarth paper Herzog et al. (2025) that reports searching over mean and max temporal pooling strategies as a hyperparameter in downstream tasks.

Table 1: **Linear probe accuracy across embedding sources.** Gap = accuracy drop from random to spatial split. Dim $\times$  reports output dimensionality relative to embedding size  $D$ ; PCA and BoVW are fixed-size outputs ( $64/D$ ,  $128/D$ ). \*OlmoEarth-Nano variant.

Pooling	Dim $\times$	Spatial split				Random split				Gap $\downarrow$
		AEF	OlmoEarth*	Tessera	Avg	AEF	OlmoEarth*	Tessera	Avg	
Mean	1 $\times$	83.9	75.7	82.2	80.6	95.4	82.3	94.2	90.7	10.0
Center-Weighted	1 $\times$	84.8	76.0	83.3	81.4	96.2	83.1	94.5	91.3	9.9
Std	1 $\times$	76.4	87.5	86.1	83.3	90.8	92.9	95.1	93.0	9.6
Max	1 $\times$	86.0	84.0	82.9	84.3	92.8	87.0	90.6	90.1	<b>5.8</b>
Median+IQR	2 $\times$	82.0	87.0	85.5	84.8	94.8	91.6	94.9	93.8	9.0
GeM	1 $\times$	84.9	85.3	87.2	85.8	95.6	91.3	95.4	94.1	8.3
Mean+Std	2 $\times$	82.2	89.6	86.4	86.1	96.1	94.6	95.5	95.4	9.3
Percentiles	5 $\times$	84.6	89.9	87.6	87.3	96.1	94.2	<b>96.3</b>	95.5	8.2
Covariance	$\frac{D+1}{2}\times$	88.9	87.2	86.6	87.6	96.1	93.7	95.7	95.2	7.6
Mean+Max	$\frac{2}{2}\times$	88.4	88.0	87.5	87.9	<b>96.3</b>	91.8	94.9	94.3	6.4
Stats	4 $\times$	88.5	<b>90.8</b>	<b>89.2</b>	<b>89.5</b>	96.1	<b>94.6</b>	96.2	<b>95.7</b>	6.2
<i>Parametric pools (fit on train set)</i>										
BoVW	$\frac{128}{D}\times$	<b>92.3</b>	71.1	77.4	80.3	94.6	87.1	90.3	90.7	10.4
PCA	$\frac{64}{D}\times$	80.6	83.8	79.8	81.4	95.4	92.3	92.2	93.3	11.9

**Distributional statistics** ( $D$ -d to  $5D$ -d): *std* captures pixel variability; *mean+std* ( $2D$ -d) and *mean+max* ( $2D$ -d) concatenate complementary signals; *stats* ( $4D$ -d) stacks min/max/mean/std; *percentiles* ( $5D$ -d) computes the (10th, 25th, 50th, 75th, 90th) percentiles; *median+IQR* ( $2D$ -d) provides robust location and spread estimates; *covariance* extracts the upper triangle of the pixel covariance matrix ( $D(D+1)/2$ -d).

**Parametric methods** (fit on known training set): *PCA* projects mean-pooled embeddings to lower dimensions (e.g., 32-d or 64-d); *Bag of Visual Words (BoVW)* (Csurka et al., 2004) clusters pixel embeddings with mini-batch  $k$ -means (128 clusters) and represents each patch as a normalized histogram of cluster assignments. These require fitting and can overfit training data structure. We include them to contrast training-free pooling with learned alternatives which require a known train holdout set.

## 4 EXPERIMENTAL SETUP

We evaluate with two probes: kNN ( $k=5$ , cosine distance) as a similarity-based proxy, and multinomial logistic regression (L-BFGS, default `scikit-learn` parameters) for discriminative classification. kNN probes geometry; linear probes test linear separability. We standardize before linear probing while kNN normalizes implicitly via cosine distance. We evaluate on both random and geographically disjoint (spatial) splits. Results are reported in Tables 1, 2. Code is available at <https://github.com/isaacacorley/geopool>.

## 5 RESULTS

**Distributional statistics improve generalization.** For linear probes, *stats* pooling reaches 88–91% on spatial splits (avg 89.5%) versus 76–84% for *mean* (avg 80.6%), a +7–10% gain (Tables 1, 2). *Mean+max* performs similarly (avg 88.0%) at half the size. On random splits, differences change to 3–5% as spatial leakage boosts all methods.

kNN results reveal encoder-specific patterns. On OlmoEarth, *std* boosts kNN spatial accuracy by +11% over *mean* (75.0% vs 64.0%), though *std* underperforms *stats* for linear probes. On Tessera, *covariance* pooling performs best (81.2%). Second-order statistics help similarity search but are less linearly separable.

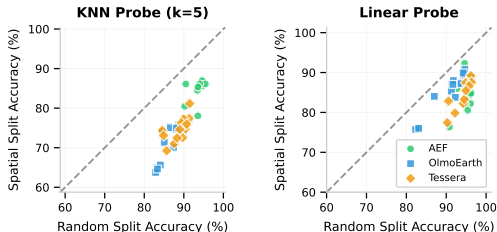


Figure 2: **Random vs spatial accuracy.** Points near the diagonal (where random = spatial) have smaller generalization gaps.

Table 2: **kNN accuracy ( $k=5$ ) across embedding sources.** Gap = accuracy drop from random to spatial split. Dim $\times$  reports output dimensionality relative to embedding size  $D$ ; PCA and BoVW are fixed-size outputs ( $64/D$ ,  $128/D$ ). \*OlmoEarth-Nano variant.

Pooling	Dim $\times$	Spatial split				Random split				Gap $\downarrow$
		AEF	OlmoEarth*	Tessera	Avg	AEF	OlmoEarth*	Tessera	Avg	
Mean	1 $\times$	85.5	64.0	71.0	73.5	94.6	83.1	87.6	88.4	14.9
Center-Weighted	1 $\times$	86.1	65.6	72.5	74.7	<b>95.4</b>	84.1	88.3	89.3	14.5
Max	1 $\times$	80.5	71.4	74.4	75.4	90.2	85.1	84.5	86.6	11.2
GeM	1 $\times$	85.8	70.1	72.5	76.1	94.6	87.4	89.7	90.6	14.4
Std	1 $\times$	78.1	75.0	77.4	76.8	93.5	86.6	91.3	90.5	13.7
Median+IQR	2 $\times$	86.1	75.0	74.6	78.6	94.0	88.1	89.0	90.4	11.8
Mean+Std	2 $\times$	86.5	74.4	74.7	78.6	94.8	90.0	90.4	<b>91.7</b>	13.1
Mean+Max	2 $\times$	85.6	75.5	76.3	79.1	94.6	88.6	89.3	90.8	11.7
Percentiles	5 $\times$	<b>86.9</b>	75.2	76.0	79.4	94.6	89.6	90.7	91.7	12.3
Covariance	$\frac{D+1}{2}\times$	84.5	74.1	<b>81.2</b>	79.9	93.4	84.6	<b>91.5</b>	89.8	<b>9.9</b>
Stats	4 $\times$	86.9	<b>76.7</b>	77.3	<b>80.3</b>	94.9	<b>90.1</b>	90.0	91.6	11.4
<i>Parametric pools (fit on train set)</i>										
PCA	$\frac{64}{D}\times$	85.4	63.8	69.2	72.8	93.6	82.9	85.7	87.4	14.6
BoVW	$\frac{128}{D}\times$	86.1	64.6	73.1	74.6	90.5	83.3	84.9	86.2	11.6

**Parametric methods vary across encoders.** While *BoVW* yields the highest AEF spatial accuracy for the linear probe (92.3%), it fails on other sources (71.1% on OlmoEarth-Nano). *PCA* mirrors *mean* pooling performance when output dimension matches embedding dimension. *Stats* pooling improves all encoders without fitting on training data. The Dim $\times$  column highlights the tradeoff: *center-weighted mean* is a strong 1 $\times$  option, while *stats* reaches peak accuracy at 4 $\times$ .

**Generalization gaps.** Figure 2 shows methods diverge under distribution shift. For linear probes, *mean* pooling drops 10% (random to spatial); *mean+max* drops only 6.4%. The Gap column shows richer statistics generalize better: *stats* (6.2) and *mean+max* (6.4) are among the smallest gaps for high-performing methods, while *max* (5.8) is smallest but lower accuracy.

**Encoder sensitivity.** Pooling interacts with encoder architecture. Tessera (512-d) achieves strong random-split accuracy but also the largest gap under *mean* pooling (12%); higher-dimensional embeddings benefit most from summary statistics. AEF (64-d) shows smaller gaps, suggesting compact embeddings are more robust to distribution shift.

## 6 DISCUSSION

**Recommendation.** We recommend *Generalized Mean Pooling (GeM)* as a drop-in replacement for *mean* pooling: it achieves +5% spatial accuracy while preserving dimensionality (1 $\times$ ), requiring no retraining or storage overhead. For maximum accuracy, *stats* pooling (4 $\times$ ) or *mean+max* (2 $\times$ ) offer further gains; for kNN retrieval, *covariance* or *percentiles* are reliable.

**Why distributional statistics help.** *Mean* pooling collapses each patch to a first-moment summary, discarding intra-patch heterogeneity; this is brittle under spatial splits where train and test regions experience distribution shifts in reflectance and composition. Higher-order distributional statistics (e.g., covariance and other moments/quantiles) preserve variability between rooftops, roads, and vegetation that can separate classes with similar means. This aligns with image-retrieval results (Radenović et al., 2018), where *GeM* outperforms *mean* pooling.

**Role of embedding dimension.** Recommendations hold across 64–512 dimensions, but improvement magnitude varies. Tessera (512-d) shows the largest *mean*-pooling gap (12%), suggesting higher-dimensional embeddings benefit most from summary statistics. AEF (64-d, int8) shows smaller gaps, indicating compact embeddings are more robust to distribution shift.

**Limitations.** We evaluate on a single benchmark (EuroSAT, 10 classes) with three embedding sources; broader coverage across datasets (BigEarthNet, fMoW) and multi-label settings would strengthen conclusions. We focus on training-free pooling; learned methods such as attention pooling or adaptive GeM may improve further but require task-specific training (Touvron et al., 2022). We use fixed hyperparameters ( $p=3$  for GeM,  $k=5$  for kNN) selected via preliminary sweeps; per-encoder tuning showed marginal differences.

## REFERENCES

- Christopher F Brown, Michal R Kazmierski, Valerie J Pasquarella, William J Rucklidge, Masha Samsikova, Chenhui Zhang, Evan Shelhamer, Estefania Lahera, Olivia Wiles, Simon Ilyushchenko, et al. Alphaeart foundations: An embedding field model for accurate and efficient global mapping from sparse label data. *arXiv preprint arXiv:2507.22291*, 2025.
- Noel Cressie. *Statistics for spatial data*. John Wiley & Sons, 2015.
- Gabriella Csurka, Christopher Dance, Lixin Fan, Jutta Willamowski, and Cédric Bray. Visual categorization with bags of keypoints. In *Workshop on statistical learning in computer vision, ECCV*, volume 1, pp. 1–2. Prague, 2004.
- Burak Ekim, Girmaw Abebe Tadesse, Caleb Robinson, Gilles Hacheme, Michael Schmitt, Rahul Dodhia, and Juan M Lavista Ferres. Distribution shifts at scale: Out-of-distribution detection in earth observation. In *Proceedings of the Computer Vision and Pattern Recognition Conference*, pp. 2265–2274, 2025.
- EO4GEO. Object-based image analysis (obia) introduction. [https://eo4geocourses.github.io/PLUS\\_OBIA-Introduction](https://eo4geocourses.github.io/PLUS_OBIA-Introduction), 2026. Accessed 2026-01-28.
- Heng Fang, Adam J. Stewart, Isaac Corley, Xiao Xiang Zhu, and Hossein Azizpour. Earth embeddings as products: Taxonomy, ecosystem, and standardized access, 2026. URL <https://arxiv.org/abs/2601.13134>.
- Zhengpeng Feng, Clement Atzberger, Sadiq Jaffer, Jovana Knezevic, Silja Sormunen, Robin Young, Madeline C. Lisaius, Markus Immitzer, Toby Jackson, James Ball, David A. Coomes, Anil Madhavapeddy, Andrew Blake, and Srinivasan Keshav. Tessera: Temporal embeddings of surface spectra for earth representation and analysis, 2025. URL <https://arxiv.org/abs/2506.20380>.
- Patrick Helber, Benjamin Bischke, Andreas Dengel, and Damian Borth. Eurosat: A novel dataset and deep learning benchmark for land use and land cover classification. *IEEE Journal of Selected Topics in Applied Earth Observations and Remote Sensing*, 12(7):2217–2226, 2019.
- Henry Herzog, Favyen Bastani, Yawen Zhang, Gabriel Tseng, Joseph Redmon, Hadrien Sablon, Ryan Park, Jacob Morrison, Alexandra Buraczynski, Karen Farley, et al. Olmoeart: Stable latent image modeling for multimodal earth observation. *arXiv preprint arXiv:2511.13655*, 2025.
- Antoine Miech, Ivan Laptev, and Josef Sivic. Learnable pooling with context gating for video classification. *arXiv preprint arXiv:1706.06905*, 2017.
- Maxim Neumann, Andre Susano Pinto, Xiaohua Zhai, and Neil Houlsby. In-domain representation learning for remote sensing. *arXiv preprint arXiv:1911.06721*, 2019.
- Filip Radenović, Giorgos Toliás, and Ondřej Chum. Fine-tuning cnn image retrieval with no human annotation. *IEEE transactions on pattern analysis and machine intelligence*, 41(7):1655–1668, 2018.
- Hugo Touvron, Matthieu Cord, Alaaeldin El-Nouby, Piotr Bojanowski, Armand Joulin, Gabriel Synnaeve, and Hervé Jégou. Augmenting convolutional networks with attention-based aggregation. In *International Conference on Machine Learning*, pp. 21668–21680. PMLR, 2022.
- Scott Workman, Armin Hadzic, and M Usman Rafique. Handling image and label resolution mismatch in remote sensing. In *Proceedings of the IEEE/CVF Winter Conference on Applications of Computer Vision*, pp. 3709–3718, 2023.